THE UPGRADE OF THE ADVANCED PHOTON SOURCE*

M. Borland[†], M. Abliz, N. Arnold, T. Berenc, J. Byrd, J. Calvey, J. Carter,
J. Carwardine, H. Cease, Z. Conway, G. Decker, J. Dooling, L. Emery, J. Fuerst,
K. Harkay, A. Jain, M. Jaski, P. Kallakuri, M. Kelly, S.H. Kim, R. Lill, R. Lindberg,
J. Liu, Z. Liu, J. Nudell, C. Preissner, V. Sajaev, N. Sereno, X. Sun, Y. Sun,
S. Veseli, J. Wang, U. Wienands, A. Xiao, C. Yao, ANL, Argonne, IL 60439, USA
A. Blednykh, BNL, Upton, NY 11973, USA

Abstract

After decades of successful operation as a 7-GeV synchrotron radiation source, the Advanced Photon Source is pursing a major upgrade that involves replacement of the storage ring with an ultra-low emittance multi-bend achromat design. Using a seven-bend hybrid multi-bend achromat with reverse bending magnets gives a natural emittance of 42 pm operated at 6 GeV. The x-ray brightness is predicted to increase by more than two orders of magnitude. Challenges are many, but appear manageable based on thorough simulation and in light of the experience gained from world-wide operation of 3rd-generation light sources. The upgraded ring will operate in swap-out mode, which has allowed pushing the performance beyond the limits imposed by conventional operation.

INTRODUCTION

The Advanced Photon Source (APS) storage ring will be upgraded using a multibend achromat (MBA) [1] lattice to provide dramatically enhanced hard x-ray brightness and coherent flux. To accomplish this, a hybrid seven-bend achromat lattice has been developed, patterned after the European Synchrotron Radiation Facility (ESRF) design [2], but with the addition of reverse-direction bending magnets [3,4] ("reverse bends"). All existing insertion device (ID) and bending magnet beamline ports will be preserved. Operation with relatively high single-bunch current will be preserved, with 4.2 mA per bunch in a uniformly-spaced 48-bunch fill pattern.

The new ring has several novel features, including nearly round beams. New particle- and x-ray beam position monitors and feedback systems will be used to provide ultra-stable operation commensurate with the significantly smaller horizontal beam size. To accommodate the reduced dynamic acceptance (DA) resulting from very strong focusing, the on-axis "swap-out" [5–7] injection scheme has been chosen. In contrast to top-up [8], swap-out involves wholesale replacement of individual bunches, imposing unique requirements on the injector [9].

Table 1 shows basic parameters of the design [10]. Figure 1 compares average x-ray brightness for the present APS to various possible insertion devices in APS-U. An improvement by a factor of $10^2 \sim 10^3$ is seen up to and beyond 100

keV. Use of superconducting undulators [11] contributes significantly to the brightness increase.

Table 1: Beam Parameter Comparison

| Quantity	APS	APS-U
Beam Energy (GeV)	7	6
Beam Current (mA)	100	200
Number of Bunches	24	48
Bunch Duration (rms) (ps)	34	104
Energy Spread (rms) (%)	0.095	0.156
Bunch Spacing (ns)	153	77
Emittance Ratio	0.013	1
Horizontal Emittance (pm-rad)	3100	31.9
Horizontal Beam Size (rms) (μm)	275	12.6
Horizontal Divergence (rms) (μrad)	11	2.5
Vertical Emittance (pm-rad)	40	31.7
Vertical Beam Size (rms) (μm)	10	7.7
Vertical Divergence (rms) (μrad)	3.5	4.1
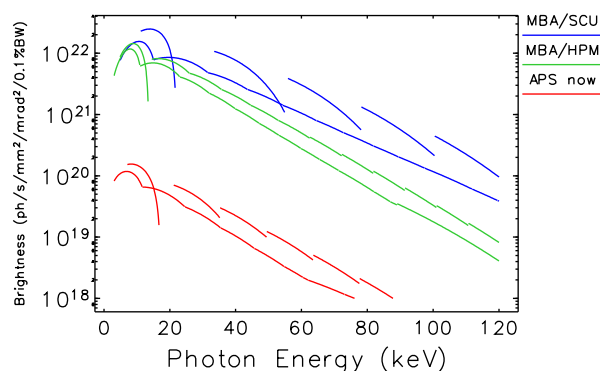
Figure 1: Brightness for several present-day APS insertion devices compared to four possible undulators in APS-U.

The paper begins with a description of the lattice design and optimization. Subsequent subsections cover commissioning simulation, collective effects, bunch-lengthening, beam lifetime, etc. Many technical challenges inherited from the aggressive physics design have been investigated through an intensive R&D program. Some of the results of that program are also presented.

02 Photon Sources and Electron Accelerators

A05 Synchrotron Radiation Facilities

BEAM PHYSICS DESIGN

Lattice Design

The essential concept for the upgrade lattice is the scaling of the natural emittance ϵ_0 with the beam energy E and the number of dipoles N_d in the ring [12]: $\epsilon_0 \sim E^2/N_d^3$. (This scaling can be explored with the Android app TAPAs [13].) What is important is not simply the number of separate dipoles, but the use of quadrupoles between the dipoles to restrain the dispersion function, reducing the degree to which quantum excitation inflates the beam emittance. Although caution must be exercised in applying this equation for different lattice structures, increasing from two (present APS) to seven dipoles per sector and reducing the energy to 6 GeV promises a 40-fold reduction in ϵ_0, from the present value of 3.1 nm to ~80 pm.

After extensive comparison with other options [14, 15], the hybrid multi-bend achromat concept [2] was adopted. Reverse-direction bending magnets [3, 4] were added, allowing reduction of the natural emittance to 42 pm [10] compared to 67 pm in the design without reverse bends [16].

As seen in Fig. 2, sextupoles are clustered within two dispersion bumps in each sector, a solution that is suited to high-energy rings as it allows significantly weaker sextupoles. The dispersion bump is optimized using five-step longitudinal gradients in the bracketing dipoles. The reverse bending magnets help decouple tuning of the dispersion and horizontal beta functions. The betatron phase advance ($\Delta\phi_x \approx 3\pi$, $\Delta\phi_y \approx \pi$) between the dispersion bumps in each sector is chosen to cancel the leading geometric sextupole effects. All of these factors are beneficial for the optimization of dynamic acceptance (DA) and beam lifetime, leading to a workable design with feasible sextupole strengths.
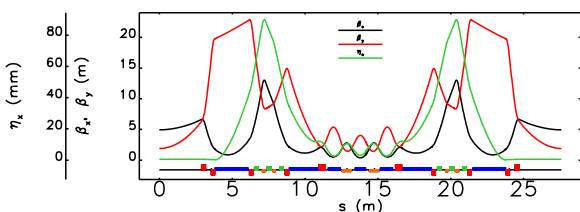

Figure 2: APS-U lattice with $\epsilon_0 = 42$ pm. Blue blocks represent normal-direction dipoles, orange blocks represent reverse-direction dipoles, red blocks represent quadrupoles, and green blocks represent sextupoles.

Nonlinear dynamics optimization used a tracking-based approach [17] that provides direct optimization of DA and Touschek lifetime (via local momentum acceptance (LMA)) using a multi-objective genetic algorithm (MOGA) similar to those described in [18,19]. The algorithm typically varied both gradients and sextupole strengths, using twelve families of sextupoles across two sectors; no symmetry was imposed on the sextupole configuration. A single function evaluation for MOGA typically consists of five steps, run in sequence on (typically) 32 cores using the programs elegant [20] and

Pelegant [21]: 1. Optional optics matching to obtain specific linear optics targets. 2. Determination of momentum-dependent tunes. 3. Generation of errors for quadrupoles and sextupoles to represent in a reasonably well-corrected lattice. 4. Determination of DA with errors. 5. Determination of LMA [22, 23] with errors at sufficient locations to support Touschek lifetime calculation.

Penalty functions are set to favor large DA with a smooth boundary, long beam lifetime, a well-controlled momentum tune footprint, and high x-ray brightness at 10 keV. Following optimization, solutions on the Pareto-optimal front are examined in detail to choose those that best balance the sometimes conflicting objectives. One or more solutions are then subjected to evaluation with a large number of error ensembles, as described in next section.

Commissioning Simulation and Lattice Evaluation

The APS-U lattice requires much stronger focusing than the present APS ring. Quadrupole misalignments generate large orbit errors, which, in the presence of very strong sextupoles, leads to large lattice and coupling errors. Combined with smaller vacuum chamber apertures—required to achieve high gradients in the magnets—this presents a significant challenge for fast commissioning.

Rigorous prediction of lattice performance in the presence of lattice and alignment errors is critical for such lattices. To simulate nonlinear dynamics with realistic errors, one needs to include orbit and lattice corrections prior to evaluation. A commissioning simulation was developed to assess whether fast commissioning is possible and to provide configurations with realistic post-commissioning errors and corrections, The commissioning simulation includes several steps: generation of displacement, tilt, and calibration errors for all elements using the errors listed in Table 2; correction of first-turn trajectory; orbit correction; beta function and coupling correction; and coupling adjustment [24]. The simulation procedure is automated, allowing running hundreds of error sets. The procedure can successfully correct orbit and optics in over 95% of cases; the remaining cases require some human intervention. The results are statistically analyzed for many parameters, e.g., orbit and lattice perturbations, corrector strength requirements, emittances, etc.

The configurations resulting from the commissioning simulation are used as input for tracking simulations that provide statistics for the dynamic acceptance, lifetime, injection efficiency, and other quantities [10]. Physical apertures, magnet systematic and random multipoles, multipoles generated by correcting elements, multipoles generated by insertion devices are all included in the evaluation. Figure 3 shows expected lifetime distributions for 100 commissioned lattices.

Collective Effects

APS-U will operate with 200 mA in as few as 48 bunches, giving up to 15.3 nC/bunch. Our assessment of collective instabilities includes careful accounting of all longitudinal and transverse impedances—reduced through re-engineering of

Table 2: RMS Values for Various Errors used for Start-to-End Lattice Commissioning Simulation. BPM stands for Beam Position Monitors.

|	
Girder misalignment	100 μm
Elements within girder	30 μm
Dipole fractional strength error	$1 \cdot 10^{-3}$
Quadrupole fractional strength error	$1 \cdot 10^{-3}$
Dipole tilt	0.4 mrad
Quadrupole tilt	0.4 mrad
Sextupole tilt	0.4 mrad
Corrector calibration error	5%
Initial BPM offset error	500 μm
BPM calibration error	5%
BPM single-shot measurement noise	30 μm
BPM orbit measurement noise	0.1 μm
BPM and corrector tilts	1 mrad
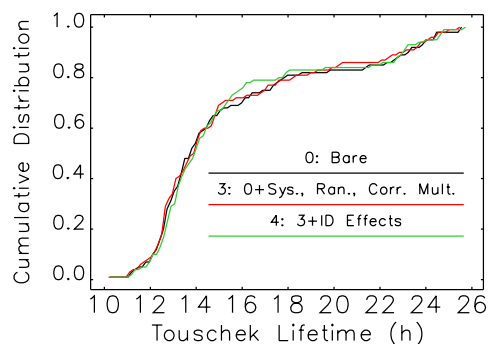
Figure 3: Cumulative distribution of approximate Touschek lifetime for 200 mA, 324 bunches, round-beam mode. Different curves show different combinations of multipoles.

vacuum chamber parts when possible—and accurate simulation of single and multiple bunches [25–27]. The resistive wall impedance is calculated analytically, while the geometrical impedance is calculated with ECHO2D [28] and GdfidL [29], using a Gaussian bunch with a 1-mm rms length (the typical rms bunch length is $\sigma_z \geq 12$ mm). Tracking is then performed with the parallel version of `elegant`.

The longitudinal impedance produces 3-fold bunch lengthening ($\sigma_z \rightarrow 12$ mm) even without the passive higher harmonic cavity (HHC). The HHC is tuned to provide $\sigma_z = 30$ mm, partly suppressing the microwave instability and increasing Touschek lifetime.

For transverse effects, the lumped element approach that works for the existing APS ring [30, 31], must be replaced with element-by-element tracking with multiple impedance elements per sector. Chromaticities of +5 ensure stability of stored bunches. However, the longitudinal mismatch between the injected beam and the ring causes the bunch to tumble in the rf bucket, which leads to longitudinal substructure and local current peaks in the injected bunch [27, 32]. Simulations show that transverse feedback or increased injected beam energy spread eliminate beam loss.

The APS-U lattice has four-fold lower longitudinal radiation damping than APS, raising concerns about longitudinal coupled bunch instability (CBI). Monte Carlo simulations [33, 34] with the resonant frequencies of the known higher-order modes (HOMs) of the 12 APS main rf cavities show a high probability of CBI unless longitudinal feedback is used. Ignoring the HHC, the simulated distribution of net longitudinal growth rates is between 0 and 150 s^{-1}, i.e., always unstable. Individual cavity temperature tuning, simulated with a simple scaling of relative frequencies with temperature, can modify this to between -20 and 100 s^{-1}.

The HHC increases synchrotron frequency spread [35], which adds damping. However, it also reduces the average synchrotron frequency, which increases the growth rates. Since the standard normal mode calculation [36] is no longer valid with the HHC present, multi-particle tracking with full longitudinal impedance model and cavity models must be used. A selection of 11 representative cases representing the full range of possible growth rates was modeled, showing 2-3 times higher growth rates, i.e., a range of 0 to 600 s^{-1}. A commercially-available longitudinal feedback system appears adequate to obtain stability. However, it appears that unconventional direct sensing of the energy error (rather than phase error) is required [37].

Transverse HOM-driven CBI was also modeled and is easily handled by conventional feedback. In contrast, fast ion instabilities could be an issue. Basic formulas [38] for ion trapping show that we need to be worried primarily with 324 bunches with round beams. Ion instability was simulated using a modified version of the ion simulation code developed at SLAC [39]. The simulations incorporate realistic vacuum profiles obtained from CERN codes SynRad+ and MolFlow+ [40, 41] for different amounts of synchrotron radiation scrubbing. The round beam case of 324 bunches produces a somewhat self-limiting instability of about 10% of vertical beam size. The well-known approach of introducing gaps in the bunch train was simulated. A gap of two bunches in two trains was seen to greatly reduce the growth rate to values that the coherent and transverse feedback damping can handle. Using more trains further reduces the growth rate. To prevent HHC transients, the last and first bunches of the train were doubled in charge. Calculations show that at the start of commissioning, when the vacuum is poorest and beam current is low, one should use a lower number of bunches to avoid ion trapping.

Beam Lifetime and Collimation

With the ultra-low emittance of the APS-U ring, Touschek lifetime will dominate as it does in third-generation rings. The gas-scattering lifetime will also be relatively short because of the small dynamic acceptance. With short lifetimes, an effective collimation system is needed to protect insertion devices and localize beam losses to easily-shielded areas.

Full Touschek lifetime evaluation [42] begins with tracking results that give the equilibrium energy spread and bunch longitudinal profile as a function of harmonic cavity detuning in the presence of the short-range wake. We evaluate

intrabeam scattering for each bunch profile [43], obtaining inflated energy spread and emittance compared to the tracking results. Suitably modified bunch profiles are then fed to `touschekLifetime` along with the 100 LMA results from ensemble evaluation, providing a statistical distribution of Touschek lifetime. These results agree well with a tracking-based computation of Touschek scattering [44], which also provides the loss distribution around the ring.

A tracking-based simulation with `elegant` was used for elastic and inelastic gas scattering, which determines the out-scattering aperture as a function of location in the ring. This is combined with location-dependent predictions of the pressure for several gas constituents to give the lifetimes, local out-scattering rates, and local loss rates. Lifetimes agree well with simpler calculations [45].

The collimation concept includes two vertical collimators located inside the first longitudinal gradient dipoles in two sectors; one of these collimators doubles as the dump for swap-out [46]. Horizontal collimators exist near the high-η_x, high-β_x points in the upstream half of five consecutive sectors; these double as beam dumps. Detailed simulations of beam aborts and Touschek scattering show that the use of five such dumps is important, as they provide both energy and multi-phase betatron collimation.

APS-UPGRADE R&D PROGRESS

Bunch-Lengthening System R&D

A passive superconducting single-cell 4-th harmonic bunch-lenghtening cavity operating at 1.408 GHz will be installed in the APS-U storage ring. The cavity will be used to increase the rms bunch length to about 110 ps and increase beam lifetime to about 3.5 h at 200 mA current in 48-bunches operation;and 9 hours in 324-bunches operation. The cavity has been built by the Argonne Physics Division [47, 48] and has reached 2 MV of rf voltage at 2 K temperature without evidence of field emission in a test cryostat. This surpasses the 1.25 MV specification from the beam physics design. Two couplers [49], rated at 20 kW each, that allow optimizing the external Q factor have also been tested. A pneumatic mechanical tuner provides a tuning range of 600 kHz, sufficient to "park" the cavity resonance between beam harmonics to minimize the effect of the cavity if desired or for diagnostic purposes. The tuner will be a part of the cavity voltage regulation loop provided by a digital low-level rf system to stabilize the rf voltage. This system will include a small rf power generator to allow setting the cavity in the absence of beam. Two concentric SiC HOM dampers [50], one at either end of the cavity assembly, provide the necessary HOM damping; these dampers were tested for up to 1 kW of heat dissipation. A rendering of the cryomodule is shown in Fig. 4.

Stripline Kicker and Septum R&D

To accommodate the small dynamic aperture of APS-U storage ring, on-axis "swap-out" injection becomes necessary. Since our injector chain only provide single-bunch
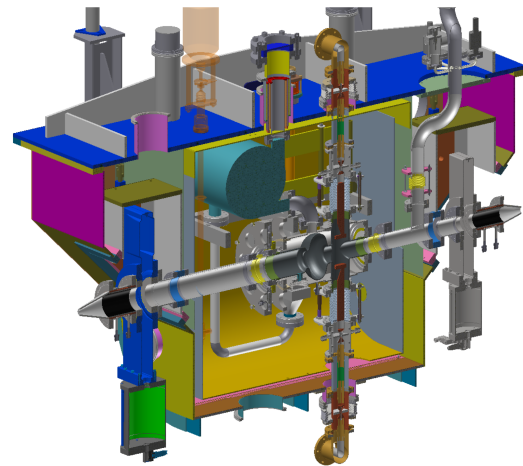

Figure 4: Harmonic cavity cryomodule. The HOM dampers are shown in black at either end of the beam pipe.The rf couplers near the cavity extend to the top and the bottom of the cryomodule, respectively.

injection, the 324-bunch high-brightness operation mode (bunch spacing of 11.4-ns) puts the most stringent demands on the high voltage pulser. Use of a single-straight injection scheme, to decouple the storage ring design and injection optimization and to avoid the strong nonlinear effects to the injected beam, raises challenges to the stripline kicker and septum magnet design. The physical requirements from a detailed physical design [51] set the stripline kicker operation voltage to be ±18-kV, and the effective field strength of septum to be 0.95-T. To ensure that such requirements can be met, a prototype stripline kicker, see Fig. 5, was built and installed in the APS booster-to-dump transport line for a test with beam. Main parameters, e.g., deflecting angle, pulse width and pulse flat-top, were measured [52,53] and all requirements satisfied. The prototype kicker was operated briefly up to ±30-kV, which far surpasses the requirement. A novel conceptual design of a Lambertson-style septum has also been made [54,55]. The calculated field quality satisfies requirements; construction of prototype magnet is underway as a collaboration between APS and FermiLab [56].
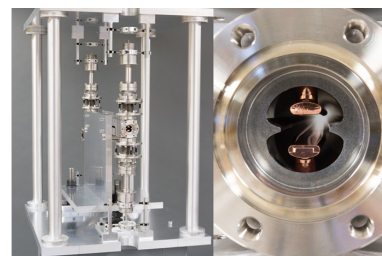

Figure 5: Prototype stripline kicker for beam test.

Ground and Girder Vibration Study

Requirements on beam orbit stability are defined as a fraction of the beam size. Due to small beam sizes in the APS-U, the orbit rms motion in 0.01-1000 Hz band is re-

quired to be below 0.4 μm in the vertical plane. To ensure that such requirements can be met, a detailed study of ground motion effects on the beam was carried out. Floor motion coherence measurements were performed in the APS tunnel, showing that the floor motion is coherent on distances up to 100 m at frequencies below 1 Hz. It was also determined through simulations that lattice amplification of the magnet displacements vanishes when displacement coherence length exceeds 50 m [57]. The effect of girder deformation modes on the orbit motion was also studied. ANSYS [58] was used to determine girder modes and their resonant frequencies. Then, `elegant` was used to calculate closed orbit distortions expected due to these girder modes. Using the measured floor motion power-spectral density spectrum, it was determined that the expected orbit motion due to girder modes should not exceed 200 nm in the horizontal and 80 nm in the vertical plane even before taking the attenuation due to orbit correction into account [59].

APS-U Fast Orbit Feedback System and R&D

The design for the APS-U fast orbit feedback system (FOFB) uses the same architecture as the present APS RTFB. A feedback controller (FBC) is located in every odd-numbered sector (20 FBCs total). The feedback controllers receive BPM values from local BPM processors turn by turn, and push them to the fast data network for distribution to the 19 other feedback controllers. There are 560 BPMs in total. Every 44.1 μsec, each feedback controller reads the latest orbit vector from the fast data network, then computes and distributes new setpoints to both fast and slow correctors in its double-sector. In total, there are 160 fast (wide-bandwidth) correctors and 320 slow correctors per plane. A block diagram of the feedback controllers is shown in Fig. 6.
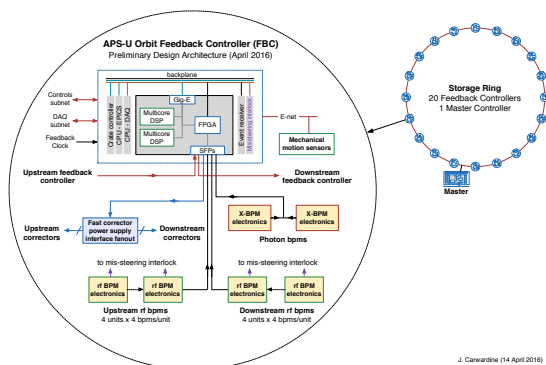

Figure 6: Fast orbit feedback architecture.

The most-recent BPM values are streamed turn-by-turn over serial fiber links. There is one link per BPM processor (corresponding to four BPMs in both planes). Setpoints for all 32 (fast and slow) corrector power supplies in the double sector are assembled into a single UDP packet that is distributed over a dedicated gigabit ethernet link to a high-performance "cut-through" network switch for distribution to the 10 corrector power supply controllers in the double

sector. The fast data network links the feedback controller with its upstream and downstream neighbors over dual bidirectional synchronous high-speed serial data links. Together, the interconnection of twenty feedback controllers forms a redundant bidirectional ring with a maximum of nine "hops" between any one FBC and all others. BPM data is distributed and pushed to DSP local memory every 7.36 μsec.

The goal for APS-U is to achieve a closed–loop bandwidth of ~1 kHz with sufficient spatial resolution to independently control each x-ray source-point. Key differences between the APS-U FOFB and the present RTFB include:

1. Four fast correctors per sector instead of one, which allows independent control of position and angle at every source point.
2. A single unified orbit feedback system using all fast and slow correctors.
3. An orbit correction sampling rate of 22.6 kHz instead of the present 1.6 kHz.
4. New corrector magnets and power supplies with fast response and wide bandwidth.

Limitations on minimizing the long-term orbit drift are entirely reliant on the quality of the measurements of the orbit trajectory through the source points. The orbit feedback system will faithfully track the readings from the beam position monitors, but without further information can do nothing to compensate for any movement of the BPM vacuum chamber. The APS Upgrade preliminary design derives a composite slow readback of beam position from multiple sensors, comprising RF BPMs around the ID source-points, photon BPMs on the beamline frontend, and mechanical-motion sensors on the rf and photon BPM vacuum chambers. An R&D program [60] with the goal of demonstrating many aspects of the APS-U system has achieved closed-loop unity-gain bandwiths of 700 Hz [61].

CONCLUSIONS

The APS is progressing rapidly toward an upgrade to a 42-pm ultra low emittance storage ring. The physics analysis is extremely detailed and the design is nearing completion. Risks and challenges have been identified, then mitigated with targeted R&D. No show-stoppers to the success of the project have been identified. Prototypes of many systems have been built, and production hardware is beginning to arrive.

ACKNOWLEDGMENTS

REFERENCES

[1] D. Einfeld *et al.*, *NIM-A*, 335:402, 1993.

[2] L. Farvacque *et al.*, *Proc. of IPAC'13*, p. 79, 2013.

[3] J. Delahaye *et al.*, *Proc. of PAC'89*, p. 1611, 1990.

[4] A. Streun. *NIM A*, 737:148, 2014.

[5] R. Abela *et al.*, *Proc. of EPAC'92*, p. 486, 1992.

[6] L. Emery *et al.*, *Proc. of PAC'03*, p. 256, 2003.

[7] A. Xiao *et al.*, *Proc. of NAPAC'13*, p. 1076, 2013.

[8] L. Emery *et al.*, *Proc. of PAC'99*, p. 200, 1999.

[9] C.-Y. Yao *et al.*, *Proc. of IPAC'15*, p. 1828, 2015.

[10] M. Borland *et al.*, *Proc. of NAPAC'16*, p. 877, 2016.

[11] Y. Ivanushenkov, et. al., *Proc. of NAPAC'16*, p. 1068, 2016.

[12] J. Murphy, BNL-42333, BNL, 1989.

[13] M. Borland, *Proc. of NA-PAC'13*, p. 1364, 2013.

[14] Y. Sun *et al.*, *Proc. of IPAC'15*, p. 1803, 2015.

[15] Y. Sun *et al.*, *Proc. of NAPAC'16*, p. 920, 2017.

[16] M. Borland *et al.*, *Proc. of IPAC'15*, p. 1776, 2015.

[17] M. Borland *et al.*, ANL/APS/LS-319, APS, 2010.

[18] K. Deb *et al.*, *IEEE TEC*, 6:182, 2002.

[19] I. Bazarov *et al.*, *Phys. Rev. ST Accel. Beams*, 8:034202, 2005.

[20] M. Borland, ANL/APS LS-287, Advanced Photon Source, 2000.

[21] Y. Wang *et al.*, *AIP Conf. Proc.*, 877:241, 2006.

[22] C. Steier *et al.*, *Phys. Rev. E*, 65:056506, 2002.

[23] M. Belgrounne *et al.*, *Proc. of PAC'03*, p. 896, 2003.

[24] V. Sajaev *et al.*, *Proc. of IPAC15*, p. 553, 2015.

[25] R. R. Lindberg *et al.*, *Proc. of IPAC'15*, p. 1825, 2015.

[26] R. R. Lindberg *et al.*, *Proc. of IPAC'18*, paper TUPJE077, these proceedings.

[27] M. Borland *et al.*, *Proc. of ICAP15*, p. 61, 2015.

[28] I. A. Zagorodnov *et al.*, *Phys. Rev. ST Accel. Beams*, 8:042001, 2005.

[29] W. Bruns, *Proc. of LINAC'02*, p. 418, 2002.

[30] Y.-C. Chae, *Proc. of PAC'03*, p. 3017, 2003.

[31] Y.-C. Chae *et al.*, *Proc. of PAC'07*, p. 4336, 2007.

[32] R. Lindberg *et al.*, *Proc. of NAPAC'16*, p. 901, 2016.

[33] L. Emery, *Proc. of PAC'93*, p. 3360, 1993.

[34] L. Emery, *Proc. of PAC'93*, p. 4348, 2007.

[35] A. Hofmann *et al.*, CERN-ISR-TH-RF-80-26, CERN, 1980.

[36] K. Thompson *et al.*, *Phys. Rev. D*, 43:3049, 1991.

[37] L. Emery *et al.*, *Proc. of IPAC'15*, p. 1822, 2015.

[38] Y. Baconnier *et al.*, CERN/SPS/80-2, CERN, 1980.

[39] L. Wang *et al.*, *Phys. Rev. ST Accel. Beams*, 14:084401, 2011.

[40] M. Ady *et al.*, *Proc. of IPAC'14*, p. 2348, 2014.

[41] R. Kersevan, *Proc. of PAC'93*, p. 3848, 1993.

[42] A. Xiao *et al.*, *Proc. of IPAC'15*, p. 559, 2015.

[43] A. Xiao, *Proc. of Linac'08*, p. 296, 2008.

[44] A. Xiao *et al.*, *Phys. Rev. ST Accel. Beams*, 13:074201, 2010.

[45] M. Borland *et al.*, *Proc. of IPAC'15*, p. 546, 2015.

[46] M. Borland *et al.*, *Proc. of IPAC'18*, paper TUPMK004, these proceedings.

[47] S. Kim *et al.*, *Proc. of IPAC'15*, p. 1819, 2015.

[48] M. Kelly *et al.*, *Proc. of IPAC'15*, p. 3267, 2015.

[49] M. Kelly *et al.*, *Proc. of SRF'15*, p. 1346, 2015.

[50] S. Kim *et al.*, *Proc. of SRF'15*, p. 1293, 2015.

[51] A.Xiao, *Proc. of IPAC'18*, paper TUPMF017, these proceedings.

[52] C. Yao *et al.*, *Proc. of NAPAC'16*, p. 950, 2017.

[53] J. Wang, A. Xiao, X. Sun *et al.*, AOP-TN-2017-027, 2017.

[54] M. Abliz *et al.*, *Proc. of NAPAC'16*, p. 1231, 2017.

[55] M. Abliz *et al.*, *Nuclear Instruments and Methods A*, 886:7, 2018.

[56] H. Cease *et al.*, Private communication.

[57] V. Sajaev *et al.*, *Proc. of IPAC'18*, paper TUPMF012, these proceedings.

[58] www.ansys.com ANSYS – Engineering simulations and 3D design software, 2018.

[59] V. Sajaev *et al.*, *Proc. of IPAC'18*, paper TUPMF011, these proceedings.

[60] R. Lill *et al.*, *Proc. of IBIC'16*, p. 55, 2016.

[61] N. Sereno *et al.*, *Proc. of IPAC'18*, paper WEPAF007, this conference.